ChemElectroChem

Research Article
doi.org/10.1002/celc.202400574

Chemistry Europe
European Chemical Societies Publishing

www.chemelectrochem.org

Investigation of Fe(II) Complexes with 1,10-Phenanthroline and 2,2′;6′,2″-Terpyridine for Aqueous Flow Battery Applications

Jenna Hannonen,[a] Ali Tuna,[a, b] Gabriel Gonzalez,[a] Eduardo Martínez González,[a] and Pekka Peljo*[a]

Iron(II) complexes with 1,10-phenanthroline (phen) and 2,2′;6′,2″-terpyridine (terpy) ligands bearing different functional groups (methyl, 4-pyridyl, chloro, carboxylic acid) were evaluated for aqueous flow battery applications, detecting oxidation processes followed by coupled chemical reactions. Redox potentials of these compounds were sufficiently high for suitable positive electrolytes (0.88–1.29 V vs. SHE). Randles-Ševčík equation and finite element modelling with COMSOL Multiphysics were utilized in evaluating the diffusion coefficient and the apparent rates of the electron transfer and coupled chemical reactions for the compounds studied by cyclic voltammetry. The systems experience weak adsorption of reactants at glassy carbon, leading to difficulties in determining the latter kinetic parameters. Flow battery tests indicate sufficient flow battery performance with dimethyl functionalized phenanthroline complex $[Fe(II)(DMe\text{-}phen)_3]^{2+}$ with 0.06% per cycle (2.78% per day) capacity decay. However, $[Fe(II)(DMe\text{-}phen)_3]^{2+}$, as well as $[Fe(II)(phen)_3]^{2+}$, experience the discharge at two different thermodynamic conditions, suggesting dimer discharge as the source of the lower voltage plateau. The energy efficiency of $[Fe(II)(DMe\text{-}phen)_3]^{2+}$ battery was improved by cycling at higher cut-off voltage for 10 cycles, after which the lost capacity was recovered with lower cut-off voltage in one cycle. $[Fe(II)(terpy)_2]^{2+}$ had too many side reactions at lower potentials to be suitable for flow battery applications.

Introduction

In the midst of the global energy crisis, the fossil fuels need to be replaced by renewable ones. The intermittency of sun and wind energy can be addressed by integrating energy storages to the power plants to even up the high peaks of demand with the low production. Modern efforts on flow battery technology (FB) were initiated at 1974,[1] and these days FBs provide a good option for the stationary energy storage. Their power and capacity are easily scaled with the area and the number of electrochemical cells and the volume of the storage tanks. FBs can have a long cycle-lifetime and they can be sustainable with the right material selection. The state-of-the-art flow battery at the moment is vanadium flow battery (VFB), developed since the 1980s.[2] VFB uses toxic sulfuric acid solutions of vanadium redox couples in different oxidation states, which are limitedly available and therefore unpredictably priced.[3] Expanding the material selection beyond vanadium opens up more environmentally friendly and possibly more cost-effective options that are much needed.

Recently, there has been much interest in testing organic molecules and different metal complexes as electroactive materials for positive and negative FB electrolytes,[4–6] among which iron complexes[7–10] can provide relatively high redox potentials through suitable ligand design. At the moment, the best performing iron-based positive redox couple, $[Fe(II)(CN)_6]^{4-}$, was developed already in 1970s,[11] with the highest capacity retention rate (100%[12]) in controlled conditions accomplished among iron metal complexes. However, it has a rather low redox potential of 0.358 V vs. SHE[13] leading to low cell voltage. A promising approach to enhance the cell voltage of iron-based batteries is to investigate the electronic effects of organic ligand structures on the redox potential of the iron center. Ligands shifting the latter parameter toward positive values are relevant because they allow increasing the cell voltage and improving the battery output power. High cell voltages can be reached with 2,2′-bipyridine (bpy) Fe(II) complexes; $[Fe(II)(bpy)_3]^{2+}$ at 1.080 V vs. SHE and its derivation of 4,4′-placed carboxylate at 1.175 V vs. SHE.[13–15] We are interested in finding a candidate among organic ligands to improve the performance of Fe(II) metal ion electroactive material for aqueous flow batteries.

The problem with $[Fe(II)(bpy)_3]^{2+}$ is that it undergoes dimerization in the oxidized state.[16] This can be described with an EC mechanism,[17] where an electrochemical reaction (E) is followed by a chemical reaction (C). For $[Fe(II)(bpy)_3]^{2+}$ this means that the oxidation of the Fe(II) center to Fe(III) is followed

[a] J. Hannonen, A. Tuna, G. Gonzalez, Dr. E. Martínez González, Prof. P. Peljo
Department of Mechanical and Materials Engineering,
University of Turku
Turku FI-20014, Finland
E-mail: pekka.peljo@utu.fi

[b] A. Tuna
Department of Chemistry
University of Turku
Turku FI-20014, Finland

Supporting information for this article is available on the WWW under https://doi.org/10.1002/celc.202400574

by a dimerization of the Fe(III) species. The decomposition mechanism of $[Fe(II)(bpy)_3]^{2+}$/$[Fe(III)(bpy)_3]^{3+}$ has been proposed by Gao et al. to include many steps.[18] The dimerization releases ligands that could bind back to Fe(II) upon reduction of the charged state. However, the ligands can be protonated and oxidized, resulting in loss of the complexing form of the ligand and decreasing the reversibility of the dimerization process. Additionally, formation of mono- and bis-ligand Fe(II) complexes has been observed.[18] Furthermore, dimerization leads to lower energy efficiency, as the reduction potential of the dimer is significantly lower than that of the monomer, resulting in a battery that is charged at ca. 1 V and discharged at 0.5 V, when cycled *vs.* 0.15 M anthraquinone disulfonic acid (AQDS) in 1 M KCl.[19] This problem can be alleviated by preventing dimerization via replacement of one bpy ligand with two cyanides, although with slightly decreased cell voltage.[14] However, the synthesis releases toxic cyanide gas, making it a less appealing option for large scale synthesis for commercial use. Another option is to change the structure of the ligand by finding another functional group for bpy, such as CH_2OH,[18] or change the ligand design more drastically. In this paper, we have chosen the latter approach, and studied bpy-derived ligands to see if we could avoid or hinder the dimerization process of the oxidized species.

Material selection in this paper included iron(II) complexes with the 1,10-phenanthroline (phen) and 2,2′;6′,2″-terpyridine (terpy) ligands bearing different functional groups. Since these are bulkier ligands than bpy, they provide steric hinderance to the iron center. We investigated, whether dimerization or other side reactions could be avoided with these bulkier ligands. $[Fe(II)(phen)_3]^{2+}$ and $[Fe(II)(terpy)_2]^{2+}$ are known for their high redox potentials of 1.06 V vs. SHE for both in 0.5 M H_2SO_4,[20] respectively, and are open for derivations to tailor the redox potentials and solubilities to become suitable for flow battery applications. The redox potential can be easily modulated via modifications in the ligand structure; adding electron-donating or electron-withdrawing functional groups to the ligand structure allows the tuning of the redox potential, making these rather versatile structures to study as ligands. Therefore, these organic ligands with the abundant Fe element have potential to be a competitive material for developing cost-effective FBs.

The studied iron(II) complexes with phen and terpy ligands are shown in Figures 1 and 2, respectively. These configurations

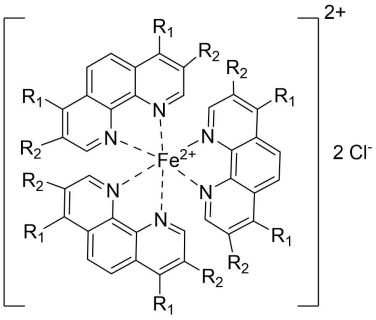

Figure 1. Structures of the studied $[Fe(II)(phen)_3]^{2+}$ with functional groups of R_1 and R_2.

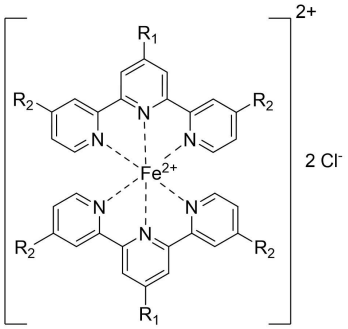

Figure 2. Structures of the studied $[Fe(II)(terpy)_2]^{2+}$ with functional groups of R_1 and R_2.

mostly lead to positively charged iron(II) complexes, unless the charges of the functional groups, such as COOH, change the overall charge of the complex to neutral or negative charge. Used functional groups are methyl (Me), 4-pyridyl (4py), carboxylic acid (COOH) and chloro (Cl). "D" indicates disubstituted and "T" tetrasubstituted functional groups in the names of the complexes. The structures of the iron(II) complexes in question were characterized with NMR and UV-Vis spectroscopy (SI). Their electrochemical behavior was studied by cyclic voltammetry (CV). CV analysis was conducted with Randles-Ševčík equation. Simulations of the cyclic voltammograms via COMSOL Multiphysics software were performed to obtain information about the kinetics of the electron transfer process of each studied complex and the chemical reaction coupled to the oxidation process. The most promising complexes were studied in a lab-scale flow battery to determine the cycling stability, where $[Fe(II)(DMe\text{-}phen)_3]^{2+}$ performed the best with a capacity decay of 0.06% per cycle (2.78% per day).

1 R_1, R_2=H

2 R_1=CH_3, R_2=H

3 R_1=R_2=CH_3

4 R_1=Cl, R_2=H

5 R_1, R_2=H

6 R_1=COOH, R_2=H

7 R_1=R_2=COOH

8 R_1=Cl, R_2=H,

9 R_1 = 4-pyridyl, R_2=H

Materials and Methods

Synthetic Procedure and Characterization

Ligand (3 eq for 1,10-phenanthroline or 2 eq for 2,2′;6′,2″-terpyridine derivatives) was dissolved into 40–45 mL of anhydrous methanol in a 100 mL beaker with a small stirring bar. The solution

was heated up to 60–65 °C and anhydrous ferrous chloride ($FeCl_2$, 1 eq) was added. Upon formation of Fe(II) complexes, color of the solution changed to deep red for Fe(II) with phen and to dark purple for Fe(II) with terpy derivatives, corresponding to the color of the final product as solid. The mixture was heated at 60–65 °C for additional 10 minutes. Afterwards, the reaction mixture was transferred to one-necked round bottom flask (100 mL) using funnel and the residue was washed with minimum amount of anhydrous methanol. The solution was slowly evaporated under reduced pressure to give the desired Fe-complexes. All phenanthroline and terpyridine derivatives and anhydrous ferrous chloride were obtained with over 97% grade from Fluorochem, UK. Anhydrous methanol was purchased from Acros Organics, Spain. More information about the synthesis is in the SI. N-alkylated azoniafluorenone (5-oxo-2-(3-(trimethylammonio)propyl)-5H-indeno[1,2-c]pyridin-2-ium bromide, **AZON3**) was prepared as described in our earlier work at University of Jyväskylä.[21]

The compounds were characterized with NMR (^1H and ^{13}C). UV-Vis spectra of the synthesis products and battery electrolytes were recorded with Specord 200 plus (analytik jena) spectrophotometer. The spectra are given in the Supplementary information (SI).

Cyclic Voltammetry (CV) and Battery Studies

CV measurements were performed in a 3-electrode cell using glassy carbon as a working electrode (3 mm diameter, BASi), Ag/AgCl as a reference electrode (3 M KCl, BASi) and platinum wire as a counter electrode by using Gamry Reference [600]+ potentiostat. Iron complex concentration was varied between 1, 2.5 and 5 mM in 0.1 M NaCl. Resistance of the solutions between the working and reference electrode was evaluated with potentiostatic impedance measurement at high frequency. Leakless Ag/AgCl reference electrode, Pt wire counter electrode and glassy carbon working electrodes (2- and 3-mm diameter, BASi) were utilized in the CV measurements performed in the storage tank during battery cycling by using PalmSens4 potentiostat.

Battery studies were performed with a LANHE Battery Testing System G340A battery cycler. Lab-scale flow battery consisted of graphite current collectors, carbon felt electrodes (thickness 4.6 mm, thermally activated, SGL) and Selemion DSVN anion-exchange membrane. Area of the cell was 5 cm^2. The iron complexes were studied as a posolyte in 0.1 M NaCl in an asymmetric flow cell versus 3-substituted N-alkylated azoniafluorenone (5-oxo-2-(3-(trimethylammonio)propyl)-5H-indeno[1,2-c]pyridin-2-ium bromide, AZON3),[21] whose stability between pH 7 and 11 has been determined by flow battery experiments.[21] The concentration of the posolytes during battery studies was 5 mM (15 ml) $[Fe(II)(phen)_3]^{2+}$, $[Fe(II)(DMe\text{-}phen)_3]^{2+}$ and $[Fe(II)(terpy)_2]^{2+}$ in 0.1 M NaCl. The negolyte (AZON3) was in excess (5 mM, 30 ml). pHs of negolyte and posolyte were adjusted to 7 prior to the battery cycling. Charge-discharge cycling was performed with constant current (CC) unless mentioned otherwise.

CV Analysis and Finite Element Method Simulation and Considered Decomposition Mechanisms

COMSOL Multiphysics software was used to build a model of the electron transfer process of the cyclic voltammogram, similar to our earlier work with iron bipyridines.[15] This model is explained in detail in SI. As experimental CVs of compounds show smaller reduction currents than expected, the mechanism can be considered as electrochemical oxidation followed by chemical reaction, or EC mechanism. This mechanism was implemented in the model, considering both first- and second-order chemical reactions, and simulations were utilized to evaluate the diffusion coefficients D_O as well as the different rate constants. Charge transfer coefficient alpha was approximated to 0.5[17] as symmetric energy barrier was expected. The diffusion coefficients were re-evaluated in the CV analysis with the Randles-Ševčík equation based on the oxidation peak currents. This CV analysis is also presented in SI.

The assumed decomposition mechanism includes the steps presented below in Equations (i)–(vii), as these are expected steps for a structurally similar compound, $[Fe(II)(bpy)_3]^{2+}$, suggested by Gao et al.[18] $[Fe(II)(phen)_3]^{2+}$ is expected to behave similarly. L represents a bidentate ligand. $[Fe(II)(terpy)_2]^{2+}$ is assumed to have ligand dissociation and dimerization in a similar manner, considering the tridentate nature of the ligand, hence enabling up to 3 free coordination sites at the iron center during ligand dissociation and dimerization. This can lead to more possibilities with both water molecule and chloride being able to act as ligands (aqueous 0.1 M NaCl as electrolyte) leading to further variation in the presented molecules in terms of the dimer ligand design.

Electron transfer reaction (i):

$$\left[Fe^{(II)}L_3\right]^{2+} \overset{k^0}{\rightleftarrows} \left[Fe^{(III)}L_3\right]^{3+} + e^- \quad \text{(i)}$$

Side reaction for Fe(II) species is ligand dissociation (ii), releasing protonated ligands.

$$\left[Fe^{(II)}L_3\right]^{2+} + H^+ + 2\ Cl^- \rightarrow \left[Fe^{(II)}L_2\right]Cl_2 + H(L)^+ \rightarrow \left[Fe^{(II)}L_1(OH_2)_2\right]Cl_2 + H(L)^+ \quad \text{(ii)}$$

Side reactions for Fe(III) include dimerization (iii-iv) and self-discharge of Fe(III) species to Fe(II) accompanied by oxidation of the free protonated ligand (vi). Dimer can be reduced back electrochemically (v). Dimerization can occur with water or chloride ions as ligands in the dimer, here one option is presented with water molecules as in ref [19].[19] Chloride ions could also be presented as ligands as in ref [18],[18] changing the charge of the dimer to +2 and releasing chloride ions when dimer is reduced. μ marks the bridging molecule (oxygen in this case) between the Fe(III) centers.

$$\left[Fe^{(III)}L_3\right]^{3+} + H_2O \rightarrow \left[Fe^{(III)}L_3(OH)\right]^{2+} + H^+ + Cl^- \rightarrow \left[Fe^{(III)}L_2Cl(OH)\right]^{+1} + HL^+ \quad \text{(iii)}$$

$$2\left[Fe^{(III)}L_2Cl(OH)\right]^{+1} + H_2O \rightarrow \mu - O - \left[Fe^{(III)}L_2(H_2O)\right]_2^{4+} + Cl^- \quad \text{(iv)}$$

$$\mu - O - \left[Fe^{(III)}L_2(H_2O)\right]_2^{4+} + 2\ HL^+ + 2\ e^- \rightarrow 2\left[Fe^{(II)}L_3\right]^{+2} + 2\ H_2O \quad \text{(v)}$$

$$2\left[Fe^{(III)}L_3\right]^{3+} + HL^+ + H_2O \rightarrow 2\left[Fe^{(II)}L_3\right]^{2+} + H(L-O)^+ + 2\ H^+ \quad \text{(vi)}$$

The ligand can be protonated as presented below:

$$L + H^+ \rightarrow HL^+ \quad \text{(vii)}$$

Fitting of the simulated data to the experimental data was performed by evaluating k^0 value based on the peak placement in the potential axis. After this, the D_O value was obtained by matching the oxidation current of the modelled CV to fit the experimental values as the concentration and number of electrons (1) were known. Finally, the k_c value (chemical reaction rate) was used to fit the simulated CV to the experimental reduction peak current. This was considered as an apparent first order reaction (k_{c1}) for ligand dissociation as well as apparent second order reaction (k_{c2}), considered due to dimerization reactions of the iron bipyridines. Due to different sensitivities of the values, several scan rates were simulated (10, 25, 50, 100, 250, 500, 1000 mV/s). All obtained values per scan rate are given in SI.

Results and Discussion

Redox Potentials

Cyclic voltammograms of 1 mM iron(II) complexes in 0.1 M NaCl are presented in Figure 3, showing redox activity at positive potentials. As expected, the electron-withdrawing groups (Cl, COOH, 4py) move the redox potentials to more positive values compared with the non-substituted iron(II) complex, whereas the electron-donating substituents (Me) move the redox potential to less positive values. The electron density at the proximity of the Fe(II) center becomes more negative and it is more energetically favorable to oxidize Fe(II) at lower potentials, when electrons are donated by substituents. If the substituents are of electron-withdrawing nature, the oxidation of Fe(II) becomes harder and occurs at higher potentials. Taking the average potential of the oxidation and reduction peaks of the CVs tested at 1 mM sample in 0.1 M NaCl, half-wave potential values $E_{1/2}$ were obtained and compiled in Table 1. These data exhibited systems of suitable redox potentials for developing flow battery posolytes (0.88 to 1.29 V *vs.* SHE), with the most positive values located close to the potential at which the oxygen evolution reaction is inevitable. For some of the studied compounds, the redox potentials were also found in literature: $[Fe(II)(phen)_3]^{2+}$ 1.06 V *vs.* SHE, $[Fe(II)(DMe\text{-}phen)_3]^{2+}$ 0.93 V *vs.* SHE and $[Fe(II)(terpy)_2]^{2+}$ 1.06 V *vs.* SHE in 0.5 M H_2SO_4 [20]. These are corresponding to the obtained redox potentials in this work. pHs of the solutions are mostly between 5 and 7. COOH-groups cause the pH of the solutions to drop to 3.

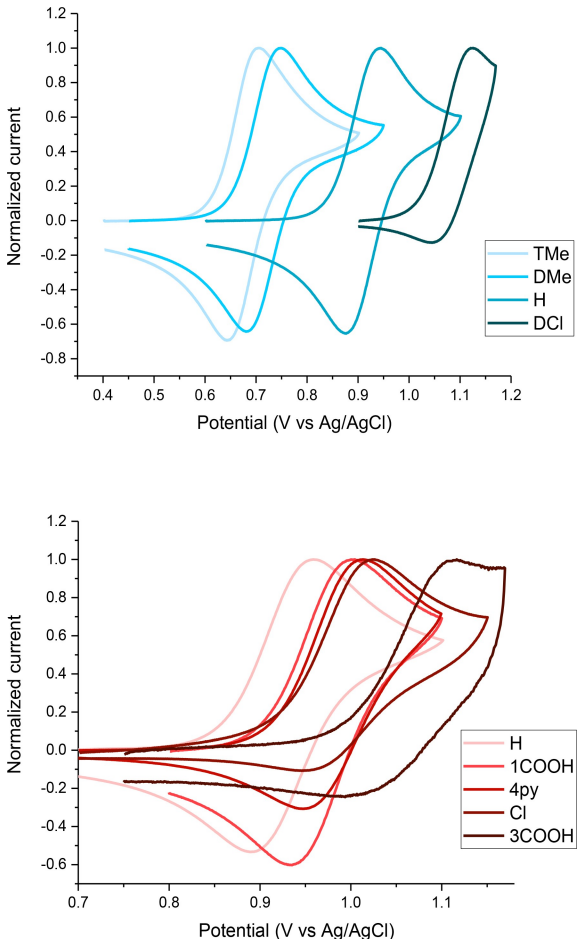

Figure 3. Cyclic voltammograms of the studied iron(II) complexes with phen (blue) and terpy (red) ligands in 0.1 M NaCl. WE glassy carbon (diameter 3 mm), scan rate 100 mV/s, current normalized. Curves are named by their ligand derivation, D meaning di-substituted and T tetra-substituted.

CV Analysis

Concentration-dependent CV experiments were performed by using solutions 1, 2.5 and 5 mM of $[Fe(II)(phen)_3]^{2+}$, $[Fe(II)(DMe\text{-}phen)_3]^{2+}$ and $[Fe(II)(terpy)_2]^{2+}$. None of the other compounds were found to be soluble enough at 1 mM concentration, except for $[Fe(II)(DCl\text{-}phen)_3]^{2+}$. However, $[Fe(II)(DCl\text{-}phen)_3]^{2+}$, along with $[Fe(II)(Cl\text{-}terpy)_2]^{2+}$ and $[Fe(II)(4py\text{-}terpy)_2]^{2+}$, had an additional oxidation process overlapping the oxidation of the redox pair, hence excluding them from the concentration-dependent studies. The CVs of $[Fe(II)(DCl\text{-}phen)_3]^{2+}$, $[Fe(II)(Cl\text{-}terpy)_2]^{2+}$ and $[Fe(II)(4py\text{-}terpy)_2]^{2+}$, show that there is an additional reduction peak at lower potentials related to this additional oxidation current. More detailed placement of the reduction peaks and corresponding CVs are given in SI, S3.

Concentration-dependent studies of $[Fe(II)(phen)_3]^{2+}$, $[Fe(II)(DMe\text{-}phen)_3]^{2+}$ and $[Fe(II)(terpy)_2]^{2+}$ show that the reduced species do not significantly adsorb on glassy carbon, but their

Table 1. Obtained redox potentials from the CVs.

Compound	$E_{1/2}$ [V *vs.* Ag/AgCl]	$E_{1/2}$ [V *vs.* SHE]
1 $[Fe(II)(phen)_3]^{2+}$	0.91	1.12
2 $[Fe(II)(DMe\text{-}phen)_3]^{2+}$	0.72	0.92
3 $[Fe(II)(TMe\text{-}phen)_3]^{2+}$	0.67	0.88
4 $[Fe(II)(DCl\text{-}phen)_3]^{2+}$	1.09	1.29
5 $[Fe(II)(terpy)_2]^{2+}$	0.93	1.13
6 $[Fe(II)(COOH\text{-}terpy)_2]^{2+}$	0.97	1.17
7 $[Fe(II)(3COOH\text{-}terpy)_2]^{2+}$	1.04	1.25
8 $[Fe(II)(Cl\text{-}terpy)_2]^{2+}$	0.99	1.19
9 $[Fe(II)(4py\text{-}terpy)_2]^{2+}$	0.98	1.19

oxidized species show weak adsorption, similar to what happens with certain ferrocene derivatives.[22] In the latter case, the CV wave for the oxidation process of the material apparently follows the Randles-Ševčík trends established for diffusion-controlled systems. However, the forward peak current grew much faster than the reverse peak current, when increasing the scan rate. An alternative wave of evidencing these mixed mechanisms is by changing the concentration of electroactive material C* [23]. For $[Fe(II)(phen)_3]^{2+}$, $[Fe(II)(DMe\text{-}phen)_3]^{2+}$ and $[Fe(II)(terpy)_2]^{2+}$ systems studied, the oxidation peak current grew much faster than the reduction peak current when decreasing C* concentration, as exemplified in Figure 4 with the responses obtained for $[Fe(II)(phen)_3]^{2+}$. In other words, the normalized currents of the latter peak follow the trends established by Randles-Ševčík, but not the oxidation ones. In this type of mixed mechanisms, diffusion-controlled processes can be favored at high concentrations of C*. Therefore, to continue the analysis, we examined our systems increasing the concentration of C*, from 1 mM to 5 mM, demonstrating marginal contributions of adsorption interactions in the CV waves by changing the scan rate. This occurs because the surface of the electrode tends to become nearly saturated with increasing C* and the total adsorbed material becomes constant.[23] These figures of concentration dependent analysis are given in SI (S5).

Simulations with COMSOL and Randles-Ševčík Analysis

$[Fe(II)(phen)_3]^{2+}$, $[Fe(II)(DMe\text{-}phen)_3]^{2+}$ and $[Fe(II)(terpy)_2]^{2+}$ were studied via simulations with finite element model via COMSOL Multiphysics software. Randles-Ševčík (R-S) analysis was utilized to compare the diffusion coefficients D_O. Even though Randles-Ševčík equation is valid for reversible system, with no contribution from Ohmic drop, double layer capacitance *etc.*, it can be used for qualitative evaluation of quasi-reversible systems. COMSOL simulations, however, included the effects of quasi-reversible kinetics and the Ohmic drop, allowing more accurate evaluation of the electrochemical parameters. The compounds in question were chosen because of their high enough solubility (5 mM) to ensure that the adsorption process marginally affects the differences between the oxidation and reduction peak currents. Under this condition, it can be assumed that the system is diffusion-controlled. All the related graphs and values are in SI, S5 and S6.

Diffusion Coefficients

Table 2 shows the agreement of the evaluated diffusion coefficients D_C from COMSOL and D_{R-S} from Randles-Ševčík equation. The diffusion coefficients of the compounds correlate inversely with the size of the complex, where the lowest D_O was obtained for the biggest compound and vice versa. Regardless their larger size compared to $[Fe(II)(bpy)_3]^{2+}$, the obtained D_O values are correlating rather well with the one determined for $[Fe(II)(bpy)_3]^{2+}$ (2.89×10^{-6} cm^2/s in 0.1 M NaCl) with the same COMSOL model in our previous work.[15]

Chemical Reaction Rates

Chemical reaction rates for the 1st order reaction (ligand dissociation) and for the 2nd order reaction (dimerization) were obtained with COMSOL Multiphysics Software. Both were obtained, due to not knowing which one of the decomposition mechanisms (ligand dissociation or dimerization) would be the rate-limiting step. Unfortunately, the analysis was inconclusive, with rate constants increasing with increasing scan rate. As the rate should be independent of the scan rate, some of the underlying reactions presented earlier, such as overlapping oxidation of the ligand, affect the experimental values. Modelling of all underlying reactions is complicated by the lack of kinetic information for each process, as well as by changes in the local pH since ligand oxidation is pH dependent. The model and the obtained results are provided in the SI (S4, S6).

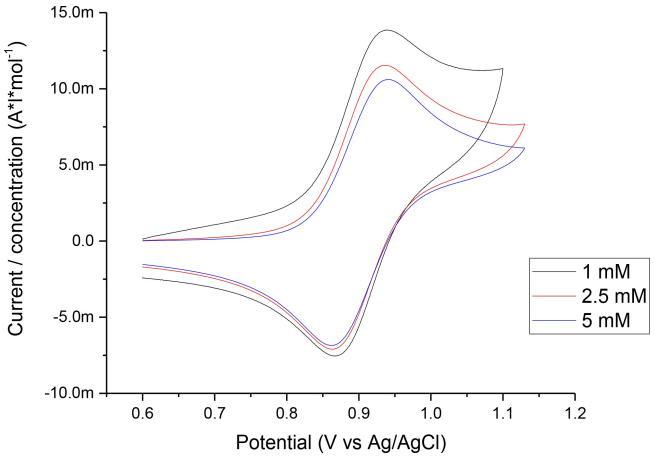

Figure 4. CVs for different concentrations of $[Fe(II)(phen)_3]^{2+}$ to demonstrate the adsorption of the oxidized species. Scan rate 100 mV/s, currents divided with the concentration.

Table 2. COMSOL results as average values of the different scan rates (10 mV/s–1 V/s) for D_C and D_{R-S} from Randles-Ševčík equation. Percentual standard deviations of D_O values in between scan rates compared to the average value, are presented in the brackets after each D_C value. Detailed information found in the SI.

Compound	10^6 D_C [cm^2/s]	10^6 D_{R-S} [cm^2/s]
1 $[Fe(II)(phen)_3]^{2+}$	3.38 (8.4%)	3.32
2 $[Fe(II)(DMe\text{-}phen)_3]^{2+}$	2.66 (6.5%)	2.62
5 $[Fe(II)(terpy)_2]^{2+}$	3.80 (8.2%)	3.68

Flow Battery Testing

[Fe(II)(phen)$_3$]$^{2+}$

[Fe(II)(phen)$_3$]$^{2+}$ was cycled as the posolyte at low concentration of 5 mM with cut-offs 0.2 V and 1.2 V to access 80% of the theoretical capacity (2 mAh). The battery exhibits large capacity decay during the first 30 cycles, losing 66% of the total accessed capacity, after which the capacity stabilizes at 0.5 mAh. Similarly to iron(II) bipyridine complex, the charging of the complex is achieved initially as one plateau, and the discharge occurs in 2–3 plateaus (Figure 5a) leading to poor energy efficiency due to the voltage drop during discharge. However, after 20 cycles, we can detect another charge plateau at lower potential (Figure 5a) than the original charge plateau. This plateau increases in capacity during cycling. From Figure 5a it is clear, that the side reaction product, which we are discharging at lower potentials, is the reason for the capacity decay we see in Figure 5b; the discharged capacity of the lower potential plateau decreases drastically, while the upper discharge plateau has much lesser decay in relation to their original values. Coulombic efficiency (CE) rises to 97.5% when the lower potential discharge plateau decreases, indicating that the side reaction product discharged at lower plateau is not completely reversible, or irreversible oxidation of ligand takes place upon charge. We cannot see the same magnitude of decay for the higher potential discharge plateau, which indicates that the Fe(III) species that do not undergo the side reaction, are more stable and present higher cycling stability.

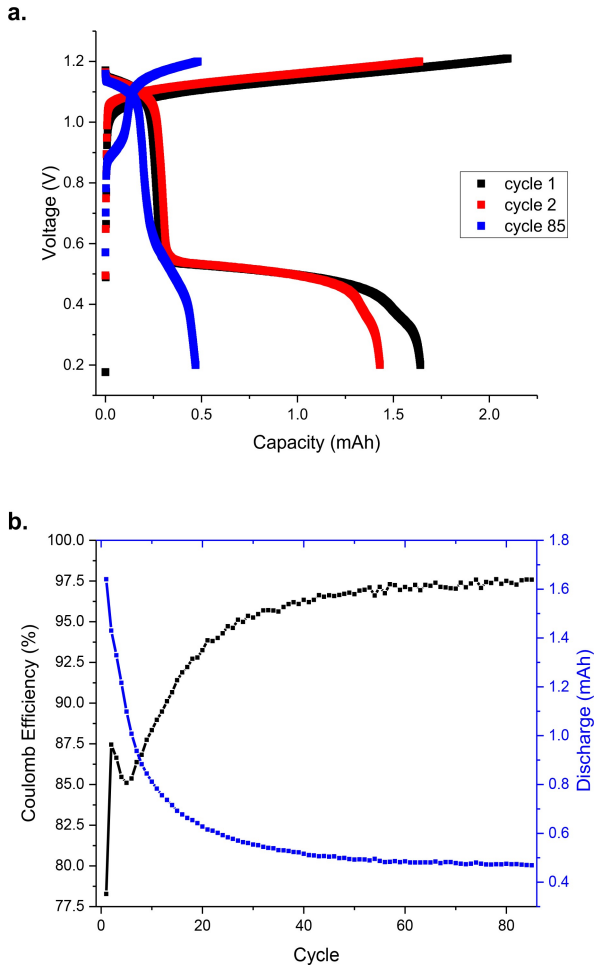

Figure 5. 5 mM [Fe(II)(phen)$_3$]$^{2+}$ battery, current density 1 mA cm^{-2}, expected capacity 2 mAh, capacity utilization 80%. **a.** capacity-voltage curves of different cycles, **b.** capacity decay and CE.

Charging in one plateau and discharging in two plateaus at different potentials is similar behavior as with [Fe(II)(bpy)$_3$]$^{2+}$, where dimerization has been proven to happen between its oxidized species, [Fe(III)(bpy)$_3$]$^{3+}$. In flow battery applications, the resulted dimer is discharged back to monomers at a lower discharge plateau.[16] As phen is a derivation of bpy, it can be assumed that the iron complexes of both these ligands have similar behavior. Therefore, dimerization interactions can also be considered for describing the reaction route of the charged species [Fe(III)(phen)$_3$]$^{3+}$, based on similar structure and similar behavior during flow battery cycling than with [Fe(II)(bpy)$_3$]$^{2+}$, especially when [Fe(III)(phen)$_3$]$^{3+}$ has been mentioned to yield μ-O-dimer.[24]

[Fe(II)(bpy)$_3$]$^{2+}$ decomposition routes would release protons initiated by dimerization.[18] We detect a pH drop in the [Fe(II)(phen)$_3$]$^{2+}$ electrolyte from 7 to 3 during battery cycling, which is below the pKa value (4.84) of phenH$^+$[25] and hence below the buffering range of the ligands, indicating proton release. Based on [Fe(II)(bpy)$_3$]$^{2+}$ decomposition route,[18] dimerization (**eq iii-iv**) and ligand oxidation (**eq vi**) can release protons, which can be used for ligand dissociation (**eq ii**) and free ligand protonation, which can lead to oxidation of the protonated ligand and further proton release (**eq vi**). Decomposition route through the ligand oxidation can be considered as a cause to low CE. The pH decrease on the posolyte side cannot be stabilized even with the negolyte pH increasing during cycling from 7 to 10, as characteristic to the negolyte.

[Fe(II)(DMe-phen)$_3$]$^{2+}$

[Fe(II)(DMe-phen)$_3$]$^{2+}$ was cycled at 5 mM concentration with constant current (CC) first by using cut-off voltages of 0.6 V and 1.05 V for 10 cycles, observing one single plateau at 1 V; however, this led to a rapid capacity decay (3.8% per cycle corresponding to 240% per day!) losing 30% of the capacity in 8 cycles (**S7.2.**). Lowering the discharge cut-off gave us an increase in capacity by accessing another discharge plateau at lower cell voltage of 0.35 V (Figure 6a) accessing 65% of the theoretical capacity of 2 mAh. This species had been produced in the first 10 charge cycles, as indicated by its large plateau size in comparison with to the following cycles. The behavior of two discharge plateaus is corresponding to the [Fe(II)(phen)$_3$]$^{2+}$ battery, as well as the pH decreasing during battery cycling. Therefore, similar decomposition mechanism is suggested to occur (eq ii–vii). The lower discharge plateau is possibly originating from the dimer discharge, however, methyl groups in the ligand might be hindering the dimerization process due to lesser size of the plateau at lower voltage compared to the [Fe(II)(phen)$_3$]$^{2+}$ battery. Additionally, accessing the lower

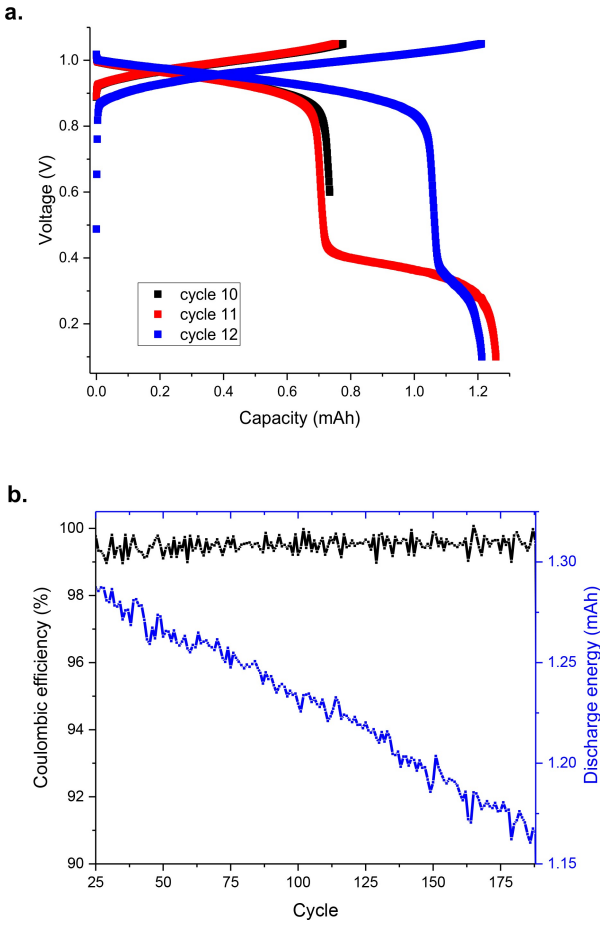

Figure 6. 5 mM $[Fe(II)(DMe\text{-}phen)_3]^{2+}$ battery, current density 1 mA cm^{-2} and expected capacity 2 mAh. **a**. charge-discharge plateaus with altering cut-offs of 0.6 V and 0.1 V for discharge, and for charge 1.05 V, **b**. discharged capacity and CE *vs.* cycle number with cut-offs 0.1–1.05 V.

discharge cut-off led to an increase in stability, resulting in a capacity decay of 0.06% per cycle (2.78% per day) (Figure 6b), being more stable than the $[Fe(II)(phen)_3]^{2+}$ battery. Capacity decay originates from the posolyte, which was ensured by removing ca. 2 ml of the charged posolyte (pH 3.5), after which the capacity decay remained the same as prior the posolyte removal. Coulombic efficiency (CE) when cycling between 0.1–1.05 V, was 99.5%.

The lower discharge potential is not beneficial in flow battery applications, therefore the iron complex was cycled between 0.6 and 1.05 V for 10 cycles, after which one cycle with cut-off for discharge was set to 0 V, to see if the monomer could be recovered. This protocol allows higher energy efficiency by improving the voltage efficiency, while still recovering the capacity using lower discharge cut-off when required. The results are presented in Figure 7. We can see that the capacity decay, when using a cut-off voltage of 0 V, is 0.65% per cycle (5.36% per day), whereas using higher cut-off of 0.6 V the capacity decay is 2.56% per cycle (200% per day!) with clear instability of the compound with these cycling cut-offs. The considerably higher capacity decay arises from not accessing the second discharge plateau at lower voltage.

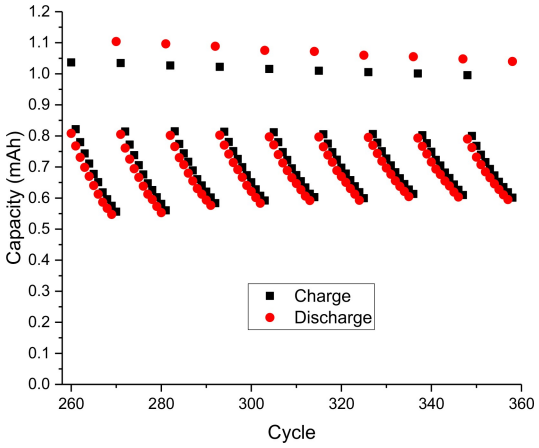

Figure 7. Capacity of the $[Fe(II)(DMe\text{-}phen)_3]^{2+}$ battery when 10 cycles are cycled at 0.6–1.05 V and 1 cycle in between to recover the capacity with a lower discharge cut-off of 0 V.

After cycling the battery with constant current (CC) (Figure 7), a combination of constant current and constant voltage (CCCV) steps (S7.2.) was tested. When using a CCCV protocol, we can access, as expected, larger capacity utilization. However, this protocol leads to longer cycling times, mainly extending the duration on the extreme state of charge, hence increasing the amount of side products. The capacity decay seems similar with the CC cycling, however, there is a new charge plateau developed at lower voltage (S7.2.) with CCCV. Considering this, CC might be a more suitable protocol for this compound to hinder the amount of the side reactions. However, total optimization of this design is not possible, due to not being able to avoid the side reactions within the operational requirements. If we could charge and discharge the battery faster than the chemical reactions occur, we could optimize this battery, however, fast discharge is not in any way practical in an energy storage application.

$[Fe(II)(terpy)_2]^{2+}$

Initially, the battery (5 mM) was cycled using cut-off voltages of 1.22 V and 0.85 V with a constant current of 1 mA cm^{-2} (Figure 8a), detecting 1 plateau for the charging and discharging process. This led to a rather rapid capacity decay (2.3% per cycle or 156% per day), which means that the capacity would have been lost in less than one day if cycling with these conditions were continued (**S7.3.**). The cutoff for discharge was lowered first to 0.4 V and later to 0 V. As a result, the discharged capacity increased exhibiting three additional discharge plateaus, which are all located at similar potentials (Figure 8a), and accessing 62% of the theoretical capacity (2 mAh). The capacity decay (0.16% per cycle, 10.1% per day) with the relatively low CE (98.5%) suggest that electrons are lost to side reactions (Figure 8b). In addition, the rising trend of the CE indicates that the lower concentration of the monomers in the solution, due to decomposition, slows down the side reactions, leading towards equilibrium.

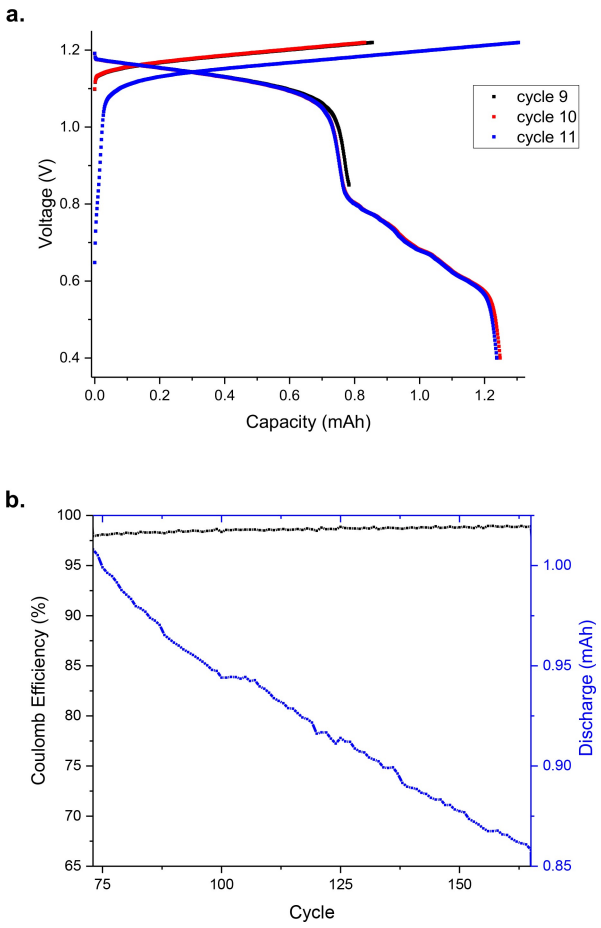

Figure 8. 5 mM $[Fe(II)(terpy)_2]^{2+}$ battery, expected capacity 2 mAh, capacity utilization 62%. **a**. Capacity-voltage curves for 1 mA cm^{-2} current density with cut-offs of 0.85 V and 0.4 V for discharge, and for charge 1.22 V, **b**. discharged capacity and CE *vs.* cycle number with cut-offs 0 and 1.22 V, current density 1 mA cm^{-2}.

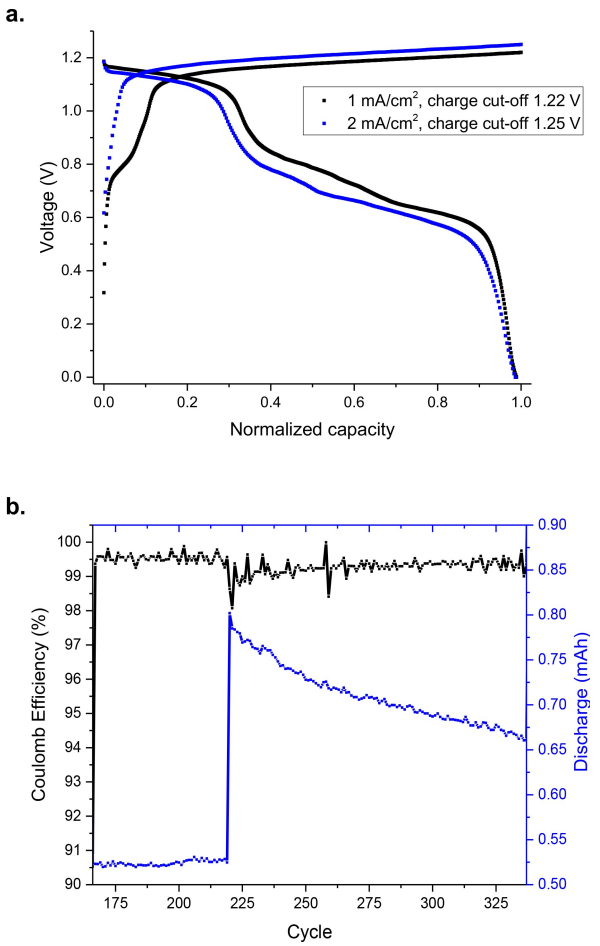

Figure 9. $[Fe(II)(terpy)_2]^{2+}$ battery **a**. Capacity-voltage curves with different current densities and charge cut-offs, capacity normalized, **b**. Coulombic efficiency and capacity *vs.* cycle number with charge cut-off 1.22 V and charge cut-off 1.25 V, current density in both 2 mA cm^{-2}.

The discharge plateaus at lower voltage and the pH drop to 4 during battery cycling (while negolyte pH increased to 8.7), indicate possible decomposition via dimerization and ligand dissociation with proton release. The process most likely differs from the suggested decomposition mechanism (eq ii–vii) due to tridentate nature of the ligand. The decomposition mechanism is hard to disclose with the information we have, since the mixture of the species is challenging to study due to not being able to fully differentiate between discharge plateaus at lower potentials.

To observe if the side reactions can be reduced due to sluggish kinetics, cycling current density was increased from 1 to 2 mA cm^{-2}. The first observation is that the charge plateau at lower potential is lost when the current density is increased (Figure 9a). Furthermore, CE increases from 98.6 to 99.5% with the increased current density, confirming that the side reactions can be hindered via higher current density cycling with no detectable capacity decay (Figure 9b). However, the higher cycling rate allows accessing a much lower capacity utilization. Then, the cut-off was increased from 1.22 to 1.25 V, leading to an increase in capacity as expected, and to a capacity decay of 0.11% per cycle (17.4% per day) while CE was 99.3% (Figure 9b). We attribute this capacity decay, after increasing the cut-off voltage, to the assessment of higher capacity utilization, which results in higher concentrations of charged species and faster side reactions.

With all this, we can say, that $[Fe(II)(terpy)_2]^{2+}$ is not suitable for flow battery applications as it is. Functional groups, such as methyl, could be suggested to make the complex bulkier and possibly hinder the side reactions by shielding the Fe(III) center upon oxidation, as seen for $[Fe(II)(DMe\text{-}phen)_3]^{2+}$ battery. However, $[Fe(II)(terpy)_2]^{2+}$ did perform better than $[Fe(II)(phen)_3]^{2+}$, showing therefore possible potential in future modification of the side groups in the structure. The studied derivations of $[Fe(II)(terpy)_2]^{2+}$ were not soluble enough nor free of side reactions based on the CV studies to be tested in a flow battery.

Comparing all of the obtained capacity decay rates with the best-performing iron complexes in the literature, we can see that our proposed complexes are not competitive. The best battery results were demonstrated by $[Fe(II)(DMe\text{-}phen)_3]^{2+}$ with a capacity decay of 0.06% per cycle (2.78% per day), while $[Fe(II)(terpy)_2]^{2+}$ and $[Fe(II)(phen)_3]^{2+}$ were more unstable. The

capacity decay of the previously mentioned symmetry-breaking iron complex $Na_4[Fe(II)(Dcbpy)_2(CN)_2]$, consisting of cyano and di-4,4'-carboxylate-bpy ligands, is 0.0016% per cycle (0.22% per day) [14] even at higher concentration of the iron complex (0.1 M). In the other work, tris(4,4′-bis(hydroxymethyl)-2,2′-bipyridine) iron dichloride *vs.* bis (3-trimethylammonio) propyl viologen tetrachloride experienced a capacity decay of 0.16% per day at approximately 0.5 M concentration.[18] Furthermore, energy efficiencies of the mentioned iron complexes of the literature, are inarguably better than of complexes presented in this work, due to discharge as one plateau instead of as multiple. Even though the cycling conditions and operational parameters and therefore the capacity decay values are not exactly comparable, they do give an idea of where the studied complexes lie in terms of capacity decay.

Flow Battery Electrolyte Characterization

The characterization of charged and discharged $[Fe(II)(phen)_3]^{2+}$ and $[Fe(II)(terpy)_2]^{2+}$ electrolytes was conducted using cyclic voltammetry and UV-Vis measurements. The charged species were electrogenerated in a flow cell following the conditions of the presented flow battery experiments. Further information is available on SI, S8.

The decomposition mechanism within studied compounds is suggested to be dimer formation as a source of the lower discharge plateaus seen during battery cycling. The CVs of the posolytes in the discharge mode after battery cycling (SI, S7) do not evidence the presence of dimers, because utilization of the lower discharge cut-off voltage led to discharge of the dimer and following formation of monomers. Therefore, the CVs were taken also at charged state on first battery cycle from the storage tank of $[Fe(II)(phen)_3]^{2+}$ and $[Fe(II)(terpy)_2]^{2+}$. Graphs are found in SI, S8. They show reduction peaks at 0.12 and 0.15 V vs. Ag/AgCl ($[Fe(II)(phen)_3]^{2+}$ and $[Fe(II)(terpy)_2]^{2+}$, respectively, ca. 700 mV lower than the iron redox pair). This corresponds to the difference between the two discharge plateaus seen in battery data (ca 600–700 mV). Similarly, $[Fe(II)(bpy)_3]^{2+}$ upon oxidation forms dimers, which are seen at a reduction peak at significantly lower potentials than the monomer reduction.[19]

The UV-Vis spectra of $[Fe(II)(phen)_3]^{2+}$ and $[Fe(II)(terpy)_2]^{2+}$ electrolytes measured in charged and discharged states suggest changes in the structure upon charge (SI, S8). The broad absorbance peak at 500 nm, characteristic to $[Fe(II)(phen)_3]^{2+}$, disappears upon charge, but without the formation of the blue $[Fe(III)(phen)_3]^{3+}$ at 600–700 nm range. This has been noted in literature with the necessary reversible reduction in regeneration of $[Fe(II)(phen)_3]^{2+}$,[24] along with the preferred formation of μ-O-dimer over $[Fe(III)(phen)_3]^{3+}$.[26] Additionally, the decreased intensity of the absorbance peak of the charged solution at 266 nm, is corresponding to the absorbance peak differences between $[Fe(II)(bpy)_3]^{2+}$ and its μ-O-dimer,[19] with the slight decrease of the wavelength of the absorbance peak at 226 nm. Therefore, the changes in the UV-Vis spectra, with the dominant dimer discharge plateau in battery cycling and the forming reduction peak at CV studies after charge, suggest dimer formation for $[Fe(II)(phen)_3]^{2+}$ upon oxidation. Furthermore, the observed brown-yellow color of the posolyte upon charge (instead of blue), is characteristic to the dimeric species[24] and supports this assumption.

In the case of $[Fe(II)(terpy)_2]^{2+}$, it also loses half of the intensity of the broad absorbance peak located at 550 nm in the UV-Vis spectrum upon charge. Intensity differences can be related to the 1:1 ratio of monomer-dimer discharged capacity during battery studies. Additionally, the absorbance peak at 319 nm decreases in intensity upon charging $[Fe(II)(terpy)_2]^{2+}$, therefore exhibiting similar behavior than $[Fe(II)(bpy)_3]^{2+}$ and its μ-O-dimer. Battery studies, reduction peak formation in CV upon charge and changes in the UV-Vis spectra can be associated to dimerization. However, the battery studies show a mixture of redox events, leading to a conclusion that the dimerization process is most likely more complicated than for $[Fe(II)(phen)_3]^{2+}$ and $[Fe(II)(bpy)_3]^{2+}$. This can be attributed to more coordination sites available upon ligand dissociation prior dimerization.

Conclusions

Derivations of phen and terpy were studied as ligand candidates for Fe(II) complexes. The obtained redox potentials (0.88 V–1.29 V *vs.* SHE) of the studied complexes are sufficiently high for developing positive flow battery electrolytes. However, the solubility of the complexes was limited in most cases, and the cyclic voltammetry also revealed some additional oxidations overlapping with the Fe oxidation for $[Fe(II)(DCl\text{-}phen)_3]^{2+}$, $[Fe(II)(Cl\text{-}terpy)_2]^{2+}$ and $[Fe(II)(4py\text{-}terpy)_2]^{2+}$. Furthermore, at low concentration of analyte C* (1 mM and 2.5 mM), CV also revealed weakly adsorption of reactants at the working electrode for $[Fe(II)(phen)_3]^{2+}$, $[Fe(II)(DMe\text{-}phen)_3]^{2+}$ and $[Fe(II)(terpy)_2]^{2+}$. Additionally, diffusion-controlled systems were evidenced at 5 mM of C*. The simulations of CVs obtained at the latter concentration for $[Fe(II)(phen)_3]^{2+}$, $[Fe(II)(DMe\text{-}phen)_3]^{2+}$ and $[Fe(II)(terpy)_2]^{2+}$ revealed diffusion coefficient values D_O of $3.38x10^{-6}$, $2.66x10^{-6}$ and $3.80x10^{-6}$ cm^2/s, respectively. To correctly evaluate the kinetics of the coupled chemical reaction, the diffusion-controlled models used for simulations should also consider the contribution of the weakly adsorption of reactants.

Energy efficiency during the battery studies was affected by a voltage drop; part of the discharge occurred at lower potential due to side reactions occurring to Fe(III) species. $[Fe(III)(phen)_3]^{3+}$ and $[Fe(III)(DMe\text{-}phen)_3]^{3+}$ experienced the discharge in 2 plateaus and $[Fe(III)(terpy)_2]^{3+}$ in 3–4 overlapping plateaus. For $[Fe(II)(DMe\text{-}phen)_3]^{2+}$ the discharge plateau at lower potential was significantly smaller than for the others, leading to lowest capacity decay among the studied compounds: 0.06% per cycle (2.78% per day) with 99.5% CE. Decomposition mechanism due to pH drop, additional discharge plateaus at lower potentials, posolyte CVs during charged state and changes in UV-Vis spectra indicate dimerization for Fe(III) species. The steric hinderance of the studied ligands and functional groups was not enough to keep the

Fe(III) center safe from side reactions. Therefore, the performance of these batteries as they are, is not adequate for practical flow batteries in terms of voltage drop via molecular stability. Further functional group design and work with different strategies are needed to decrease the side reactions and make these compounds adequate for flow battery applications.

Acknowledgements

Dr. Maxime Artault and Prof. Petri Pihko from University of Jyväskylä are gratefully acknowledged for providing the AZON3 utilized as the negative electrolyte in the battery tests. We gratefully acknowledge the financial support from Technology Industries of Finland Centennial Foundation and Jane and Aatos Erkko Foundation through the Future Makers program for the project Digipower. This project has received funding from the European Union – NextGenerationEU instrument and is funded by Research Council Finland under grant number 348326 (P.P.). G.G. gratefully acknowledges the financial support from the University of Turku Graduate School. P.P. gratefully acknowledges the Academy Research Fellow funding (grant no. 315739, 343791, 320071, and 343794) from Research Council of Finland, and European Research Council through a Starting grant (agreement no. 950038). Materials Analysis and Research Infrastructure (MARI) and Turku Centre for Chemical and Molecular Analytics (CCMA) of the University of Turku were utilized in this work.

Conflict of Interests

The authors declare no conflict of interest.

Data Availability Statement

The data that support the findings of this study are available from the corresponding author upon reasonable request.

Keywords: aqueous redox flow battery · electrochemistry · energy storage · iron complex · ligand design

[1] L. H. Thaller, *Electrically Rechargeable Redox Flow Cells*, 9th Intersociety Energy Conversion Engineering Conference. **1974**, pp. 924–928.
[2] M. Skyllas-Kazacos, M. Rychcik, R. G. Robins, A. G. Fane, M. A. Green, *J. Electrochem. Soc.* **1986**, *133*, 1057–1058. https://doi.org/10.1149/1.2108706.
[3] C. Minke, U. Kunz, T. Turek, *J. Power Sources* **2017**, *361*, 105–114. https://doi.org/10.1016/j.jpowsour.2017.06.066.
[4] W. Wang, Q. Luo, B. Li, X. Wei, L. Li, Z. Yang, *Adv. Funct. Mater.* **2013**, *23*, 970–986. https://doi.org/10.1002/adfm.201200694.
[5] R. W. Hogue, K. E. Toghill, *Curr. Opin. Electrochem.* **2019**, *18*, 37–45. https://doi.org/https://doi.org/10.1016/j.coelec.2019.08.006.
[6] M. Shoaib, P. Vallayil, N. Jaiswal, P. Iyapazham Vaigunda Suba, S. Sankararaman, K. Ramanujam, V. Thangadurai, *Adv. Energy Mater.* **2024**. https://doi.org/10.1002/aenm.202400721.
[7] K. Gong, F. Xu, J. B. Grunewald, X. Ma, Y. Zhao, S. Gu, Y. Yan, *ACS Energy Lett.* **2016**, *1*, 89–93. https://doi.org/10.1021/acsenergylett.6b00049.
[8] S. Belongia, X. Wang, X. Zhang, *Adv. Funct. Mater.* **2024**, *34*. https://doi.org/10.1002/adfm.202302077.
[9] G. S. Nambafu, A. M. Hollas, S. Zhang, P. S. Rice, D. Boglaienko, J. L. Fulton, M. Li, Q. Huang, Y. Zhu, D. M. Reed, V. L. Sprenkle, G. Li, *Nat. Commun.* **2024**, *15*, 2566. https://doi.org/10.1038/s41467-024-45862-3.
[10] A. Okazawa, T. Kakuchi, K. Kawai, M. Okubo, *APL Mater.* **2023**, *11*. https://doi.org/10.1063/5.0160078.
[11] G. B. Adams, Lockheed Missiles & Space Company, Inc., Electrically rechargeable battery, US Patent, 4,180,623A **1979**.
[12] M. Mouselly, H. Alawadhi, S. T. Senthilkumar, *Curr. Opin. Electrochem.* **2024**, *48*, 101581. https://doi.org/10.1016/j.coelec.2024.101581.
[13] P. Vanýsek, *CRC Handbook of Chemistry and Physics, 89th Edition*, Marcel Dekker **1978**.
[14] X. Li, P. Gao, Y. Y. Lai, J. D. Bazak, A. Hollas, H. Y. Lin, V. Murugesan, S. Zhang, C. F. Cheng, W. Y. Tung, Y. T. Lai, R. Feng, J. Wang, C. L. Wang, W. Wang, Y. Zhu, *Nat. Energy* **2021**, *6*, 873–881. https://doi.org/10.1038/s41560-021-00879-6.
[15] J. Hannonen, A. Kiesilä, U. Mattinen, P. M. Pihko, P. Peljo, *J. Electroanal. Chem.* **2023**, *950*. https://doi.org/10.1016/j.jelechem.2023.117847.
[16] N. E. Holubowitch, G. Nguyen, *Inorg. Chem.* **2022**, *61*, 9541–9556. https://doi.org/10.1021/acs.inorgchem.2c00640.
[17] A. J. Bard, L. R. Faulkner, *Electrochemical Methods: Fundamentals and Applications*, 2nd Edition, John Wiley & Sons Inc. **2001**.
[18] J. Gao, K. Amini, T. Y. George, Y. Jing, T. Tsukamoto, D. Xi, R. G. Gordon, M. J. Aziz, A. High Potential, *Adv. Energy Mater.* **2022**, *12*. https://doi.org/10.1002/aenm.202202444.
[19] N. E. Holubowitch, G. Nguyen, *Inorg. Chem.* **2022**, *61*, 9541–9556. https://doi.org/10.1021/acs.inorgchem.2c00640.
[20] Y. D. Chen, K. S. V. Santhanam, A. J. Bard, *J. Electrochem. Soc.* **1981**, *128*, 1460–1467. https://doi.org/10.1149/1.2127663.
[21] M. Artault, G. Gonzalez, P. Damlin, J. Toivola, A. Mailman, J. Hannonen, P. M. Pihko, P. Peljo, *Adv. Energy Mater.* **2024**, 2401635. https://doi.org/10.1002/aenm.202401635.
[22] N. Kurapati, P. Pathirathna, R. Chen, S. Amemiya, *Anal. Chem.* **2018**, *90*, 13632–13639. https://doi.org/10.1021/acs.analchem.8b03883.
[23] R. H. Wopschall, S. Irving, *Anal. Chem.* **1967**, *39*, 1514–1527. https://doi.org/10.1021/ac50156a018.
[24] M. M. Walczak, N. T. Flynn, *J. Electroanal. Chem.* **1998**, *441*, 43–49. https://doi.org/10.1016/S0022-0728(97)00416-6.
[25] W. M. Haynes, *CRC Handbook of Chemistry and Physics (97th ed.)*, CRC Press **2016**.
[26] J. E. Plowman, T. M. Loehr, C. K. Schauer, O. P. Anderson, *Inorg. Chem.* **1984**, *23*, 3553–3559. https://doi.org/10.1021/ic00190a024.

Manuscript received: October 14, 2024
Revised manuscript received: December 18, 2024
Version of record online: ■■, ■■

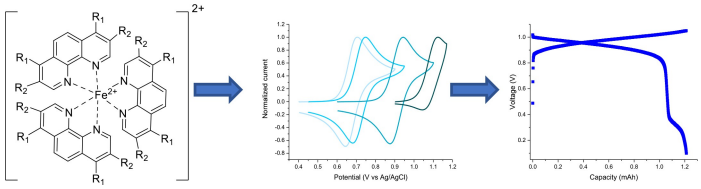

*J. Hannonen, A. Tuna, G. Gonzalez, Dr. E. Martínez González, Prof. P. Peljo**

1 – 11

Investigation of Fe(II) Complexes with 1,10-Phenanthroline and 2,2′;6′,2″-Terpyridine for Aqueous Flow Battery Applications

Iron(II) complexes with 1,10-phenanthroline (phen) and 2,2′;6′,2″-terpyridine (terpy) ligands with different substituents were evaluated for aqueous flow battery applications. Electrochemical characterization revealed suitable redox potentials (0.88–1.29 V *vs.* SHE) for positive electrolytes, however, flow battery studies revealed a voltage drop during discharge for the studied compounds, possibly originating from dimerization of the charged Fe(III) species.